J Mater Sci (2013) 48:2151–2157
DOI 10.1007/s10853-012-6990-1

Structure, dielectric, ferroelectric, and energy density properties of $(1 - x)$BZT–xBCT ceramic capacitors for energy storage applications

Venkata Sreenivas Puli · Dhiren K. Pradhan · Douglas B. Chrisey · M. Tomozawa · G. L. Sharma · J. F. Scott · Ram S. Katiyar

Received: 12 September 2012 / Accepted: 25 October 2012 / Published online: 9 November 2012

Abstract We investigate the dielectric, ferroelectric, and energy density properties of Pb-free $(1 - x)$BZT–xBCT ceramic capacitors at higher sintering temperature (1600 °C). A significant increase in the dielectric constant, with relatively low loss was observed for the investigated $\{Ba(Zr_{0.2}Ti_{0.8})O_3\}_{(1-x)}\{(Ba_{0.7}Ca_{0.3})TiO_3\}_x$ ($x = 0.10$, 0.15, 0.20) ceramics; however, electric breakdown was low (~140, 170, 134 kV/cm), and of which room temperature (300 K) charging curve energy density values are largest ~0.88, 0.94, and 0.87 J/cm^3 with maximum high dielectric constant values ~7800, 8400, and 5200, respectively. Bulk ceramic BZT–BCT materials have shown interesting energy densities with good energy storage efficiency (~72 %) at high sintering temperature; they might be one of the strong candidates for high energy density capacitor applications in an environmentally protective atmosphere.

Introduction

Materials with high dielectric constant and piezoelectric coefficients are very attractive for high energy density capacitors and actuators. Lead-based perovskite ceramics have been extensively investigated due to their high dielectric and piezoelectric properties. Recently, attention focused towards lead-free perovskite oxides, for electrical and electronic applications, of which barium titanate ($BaTiO_3$) and its solid solutions represent one of the most important dielectric and piezoelectric families. There is a great demand for electrical energy storage capacitors that can accumulate a huge amount of energy and then discharge almost instantaneously; such materials play a vital role in "pulse power" applications, mobile electronic devices, and hybrid electrical vehicles. As the requirements are growing for compact and commercially viable electronic devices, development of high power and high energy density dielectric materials are prime requisite for today's fast growing electronics industry. Capacitor dielectric materials with high energy density would help to reduce the volume, weight, and cost of power system in hybrid electric vehicles [1]. High dielectric permittivity, low loss, and high electric breakdown strength are required for energy storage capacitors in pulse power applications [2]. Dielectric ceramics and thin films categorized as linear dielectric, ferroelectric, and antiferroelectric. The reliability, fast discharge speed, low loss, high breakdown strength, and high energy density polymer dielectrics are choice of materials for energy storage. Poly(vinylidene fluoride) (PVDF) and its copolymer with trifluoroethylene (TrFE) were presently used as commercial high energy density storage capacitors with energy densities as high as >17 J/cm^3 due to higher values of breakdown field strengths (~575 MV/m), however, polymer dielectrics that are used in energy storage at present exhibits poor dielectric permittivity and their operation temperatures are rather very low [1]. On the other hand, although ferroelectric materials exhibit higher permittivity values, and find limitation due to their low breakdown voltage at higher temperatures (>200 °C) for future applications. Dielectric ceramics with high permittivity are being developed

V. S. Puli (✉) · D. K. Pradhan · G. L. Sharma · R. S. Katiyar (✉)
Department of Physics and Institute for Functional Nano Materials, University of Puerto Rico, San Juan, PR 00936, USA
e-mail: pvsri123@gmail.com

R. S. Katiyar
e-mail: rkatiyar@hpcf.upr.edu

D. B. Chrisey · M. Tomozawa
Department of Materials Science and Engineering, Rensselaer Polytechnic Institute, Troy, NY 12180-3590, USA

J. F. Scott
Cavendish Laboratory, Department of Physics, University of Cambridge, Cambridge CB0 3HE, UK

for a wide range of applications in electrical and electronics engineering, including as a dielectric for high energy density storage capacitors [2]. High energy densities are possible both in ceramics and as well as in thin film capacitors with high electric breakdown fields. $0.7BaTiO_3$–$0.3BiScO_3$ ceramics exhibit 6.1 J/cm^3 at field of 73 kV/mm [3]. Whereas linear dielectric thin films made of $Ba[(Ni_{1/2}, W_{1/2})_{0.1}Ti_{0.9}]O_3$ exhibit high energy density ~34 J/cm^3 at high breakdown field (3 MV/cm) [4]. Lead-based ferroelectric PLZT thin films exhibit an energy density of ~46 J/cm^3 at 1.3 MV/cm and antiferroelectric La-modified $PbZrO_3$ thin films reach 60 MV/m breakdown strength with energy density ~15 J/cm^3 [5, 6]. As well relaxor ferroelectric PLZT thin films grown by chemical solution deposition, have also achieved higher energy densities ~45 J/cm^3 at 3 MV/cm for potential applications such as hybrid electric drive vehicles [7]. However, it is difficult for antiferroelectric materials to withstand more than several hundred charge–discharge cycles due to cracks at their phase transitions during charge–discharge cycles [6].

The recently published lead-free BZT–BCT, BST–BCT ceramics [8, 9], with high permittivity and large piezoelectric behavior with optimal compositions at their morphotropic phase boundaries (MPB) motivated us to choose Pb-free pseudobinary ferroelectric system for energy density storage capacitor application. In this study, we therefore investigated dielectric, ferroelectric, and energy density properties of a Pb-free BZT–BCT ceramics at higher sintering temperatures.

Experimental details

All the ceramic samples were fabricated by a conventional solid-state reaction method. All the chemicals of $BaCO_3$ (99 %), $CaCO_3$ (99 %), ZrO_2 (99.7 %), and TiO_2 (97 %) were procured from Alfa Aesar, USA. The calcining was performed at 1250 °C for 10 h. Before pelletization, the calcined powders were ball milled for breaking the agglomerates. Sintering of the pellets was carried out at 1600 °C in air for 4 h. Ceramic pellets with a diameter of 13 mm and thickness of 0.5 mm were coated with silver paint as electrode, were used for electrical measurements. Temperature-dependent dielectric properties were measured using an Alfa impedance analyzer coupled with fully computer interfaced Novocontrol thermal stage with temperature range of (273–400 K) in a frequency range of 100 Hz–100 kHz. Ferroelectric hysteresis loops was measured at 50 Hz, with poled disk-shaped samples under an electric field (20 kV/cm) using Radiant Technologies high voltage amplifier (RT 6000 HVA-4000V). Dielectric breakdown voltage of the samples was measured at room temperature using a Trek high voltage amplifier (Trek Inc., Model 30 kV/20A).

Results and discussion

X-ray diffraction profiles of $(1 - x)$BZT–xBCT solid solution are presented in Fig. 1a. BZT–BCT ceramics have shown an polycrystalline perovskite crystal structure and exhibit a phase coexistence of tetragonal and rhombohedral phases, that is characterized by peak (002)/(200) splitting at around $2\theta \sim 45°$ as well as the peak (220)/(202) splitting at around $2\theta \sim 65°$–$66°$ as shown in Fig. 1a. The diffraction peaks of the samples were indexed to the perovskite-type tetragonal and rhombohedral structure were in agreement with the respective Joint Committee on Powder Diffraction Standards (JCPDS) card nos. 05-0626, 85-0368. There is no evidence of secondary phases such as $Ba_3Ca_2Ti_2O_9$ and the possibility of such impurity is minimized by sintering at higher temperatures [10]. Due to complete solid solubility of Ca^{2+} either at Ba-site or at the Ti-site and/or Zr^{4+} at Ti-site and higher sintering temperature (1600 °C), no other secondary phases were observed in the present BZT–BCT ceramics. There is a possibility of a secondary phase such as $Ba_3Ca_2Ti_2O_9$ at relatively low sintering temperatures (<1200 °C), and such an impurity phase is eliminated at higher sintering temperatures due to increased solid solubility of Ca^{2+} at the Ba-site [10]. The particle diameters were calculated by using the Scherrer's equation, for the BZT–BCT composition for (110) diffraction peak at approximately $2\theta \sim 31.47°$–$31.535°$. Calculated particle diameters were 0.92, 0.95, and 0.933 nm for $x = 0.10$, 0.15, and 0.20 BCT, respectively. Scanning electron microscopy (SEM) images are shown in Fig. 1b; dense and uniform pore-free surfaces were observed. The average grain sizes of the sintered ceramic pellets are around 20–30 μm. The measured density (g/cm^3) values were ~5.83, 5.85, and 6.00 g/cm^3, respectively, measured by Archimedes method using a pycnometer. Fine grains contributed the improvement of overall density of pellets; the average relative density of the pellets lies between ~95 and 98 % of the theoretical maximum density, suggesting that the higher sintering temperature improved the density of materials and also eliminates pores. This statement is supported in agreement to diffusion kinetics mechanism [11]. Enhanced grain growth with dense pore-free microstructure possessing highly relative densities are attributed to higher sintering temperature as well as by substitution of isovalent (Ca^{2+}, Sr^{2+}, Cd^{2+}, etc.) into Ba^{2+}, lattice anisotropy is reduced and ceramics become more dense [12]. Figure 2a shows the temperature-dependent dielectric constant behavior of $\{Ba(Zr_{0.2}Ti_{0.8})O_3\}_{(1-x)}\{(Ba_{0.7}Ca_{0.3})$-$TiO_3\}_x$ $(x = 0.10,\ 0.15,\ 0.20)$—(BZT–BCT) ceramics measured at 100 Hz–100 kHz over the temperature range of 273–470 K. For the mentioned ceramic compositions sintered at the higher temperature, the dielectric dispersion

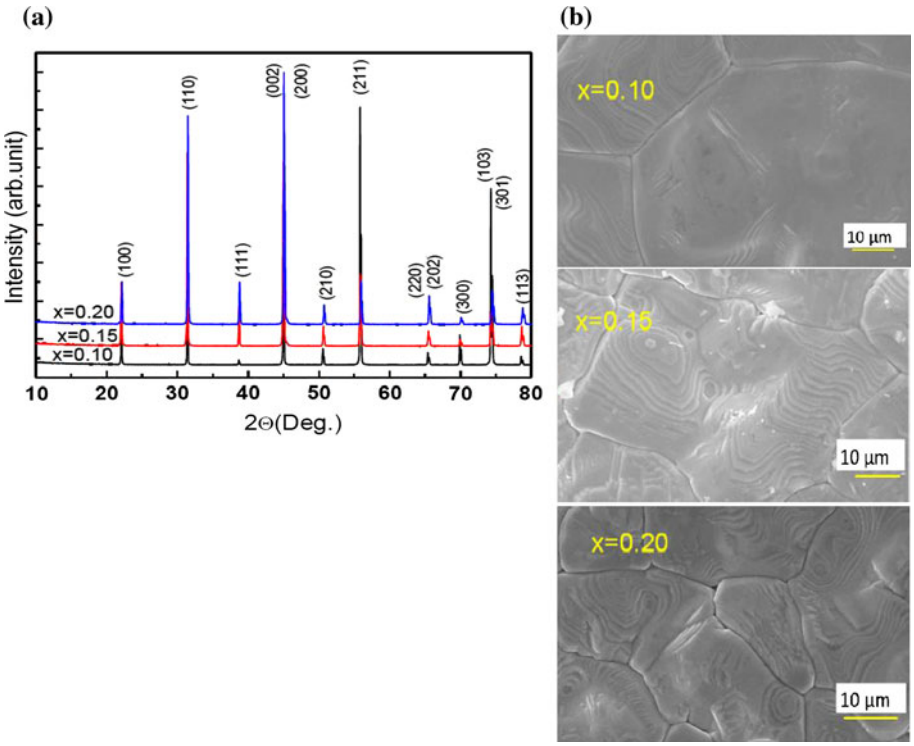

Fig. 1 **a** Room temperature XRD patterns with 2θ angle ranging from 20° to 80°. **b** SEM micrographs of $[(BaZr_{0.2}Ti_{0.80})O_3]_{(1-x)}$–$[(Ba_{0.70}Ca_{0.30})TiO_3]_x$ ($x = 0.10$, 0.15, 0.20)—(BZT–BCT) ceramics sintered at 1600 °C

becomes indistinguishable, almost throughout the temperature interval studied.

Observed Curie temperatures (T_c) for all the mentioned compositions were 310, 300, and 300 K which are far lower than that of pure $BaTiO_3$ (393 K) and of which dielectric maxima for respective compositions at room temperature are found to be ~7800, 8400, and 5200 at 100 Hz. Room temperature dielectric constant values of BZT–BCT ceramics are comparably higher than soft lead zirconate titanate (PZT) and lead-free piezoelectrics BZT–BCT [8, 13–15]. At higher sintering temperatures, the Curie temperature (T_c) decreased from 310 to 300 K, while the maximum dielectric constant increased, T_c, decrease may be attributed to increase of internal stress with increase in ferroelectric phase-free energy [16]. The decrease in phase transition temperature behavior is generally attributed to several reasons, such as intergranular stress, ferroelectric domain sizes, and the possibility of Ca^{2+} in the Ti^{4+} site, and the compositional inhomogeneity [17]. Dielectric constant values for the three compositions increases with increase in temperature and up to T_c, and then dielectric constant values started decreasing with further increase in temperature. For the BZT–BCT ceramic sintered at a given temperature, T_c does not shift with increasing frequency in the frequency interval studied. Dense microstructures with larger grains minimize the grain boundary contribution in dielectric properties. The higher values of dielectric constant (ε ~ 7800, 8400, 5200) at room temperature for BZT–BCT might be due to the enhanced grain growth which in turn arises from higher sintering temperature (1600 °C). Higher sintering temperature might be the reason for high dielectric constant values for present compositions at room temperature, when compared to the sol–gel synthesized $(1 - x)$BZT–xBCT ($x = 0.10$, 0.15, 0.20) ceramics (ε ~ 1591, 1348, 462) sintered at 1280 °C [18]. Changes in dielectric properties with change sintering temperature can be associated with a competing effect among internal stress, porosity, and grain size [16, 19]. Temperature-dependent dielectric loss (tan δ) plots are shown in Fig. 2 (inset), low dielectric loss values are in complete agreement with that of dielectric constant curves. However, for the sintered ceramics as shown in Fig. 2b, a little frequency dissipation in dielectric loss behavior measured frequencies in a wide temperature interval around T_c in dielectric constant curves. High sintering temperature might be the reason for high dielectric constant values with enhanced grain growth. Conventionally, solid-state sintered BZT–BCT ceramics exhibit higher dielectric constant values than the sol–gel synthesized BZT–BCT ceramics at low sintering temperature [1280 °C (ε_r ~ 1590)] [18]. In general, the dielectric maxima increases and Curie temperature decreases, with increasing grain size and density [20]. Increasing sintering temperature helps in grain growth, which can be explained according to the phenomenological kinetic grain growth equation [12]. The variation of dielectric constant and dielectric loss with temperature at different frequencies (Fig. 2b) followed the general trend with the increment of

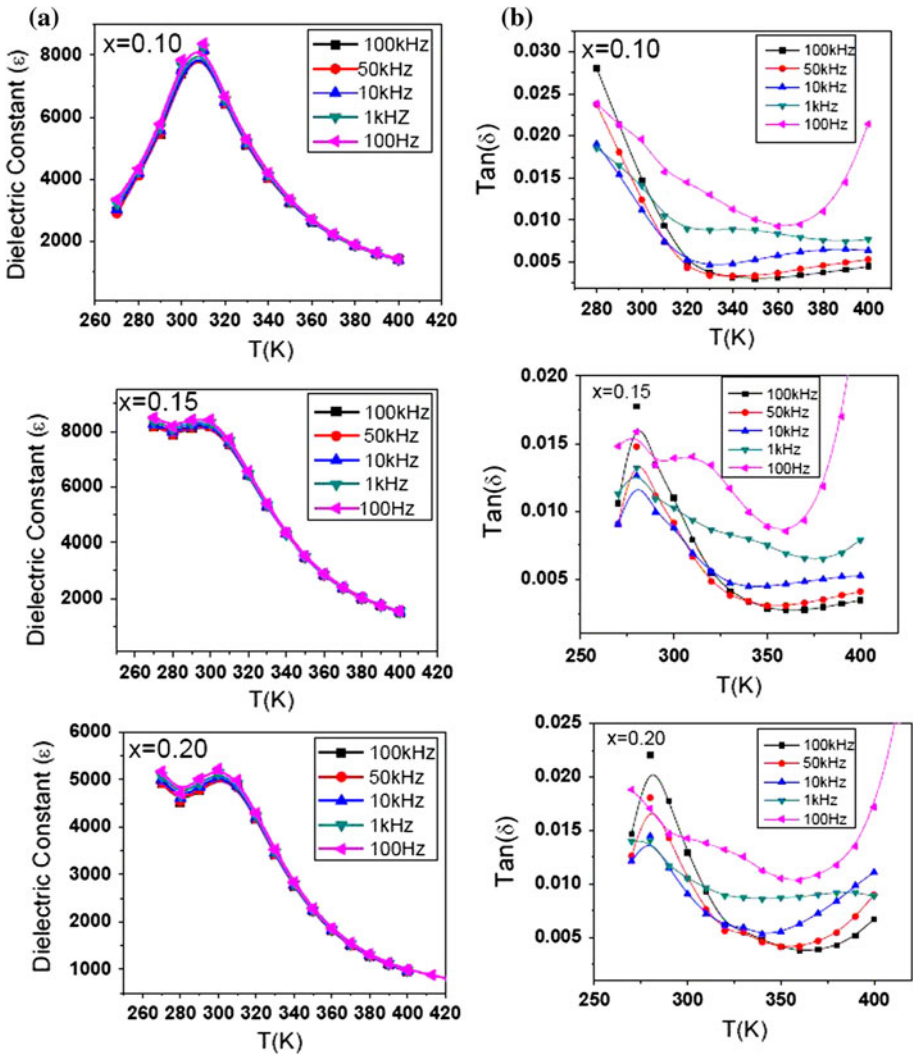

Fig. 2 **a** Temperature-dependent dielectric constant and **b** temperature-dependent dielectric loss (tan δ) of $[(BaZr_{0.2}Ti_{0.80})O_3]_{(1-x)}$–$[(Ba_{0.70}Ca_{0.30})TiO_3]_x$ ($x = 0.10$, 0.15, 0.20)—(BZT–BCT) ceramics sintered at 1600 °C (100 Hz–100 kHz)

both dielectric constant and dielectric loss (tangent loss) decrease with increasing frequency. These high dielectric constant and low loss values for the BZT–BCT composition might be due to compositional proximity ($x = 0.32$) to the C–R–T triple point in the phase diagram of $\{Ba(Zr_{0.2}Ti_{0.8})O_3\}_{(1-x)}\{(Ba_{0.7}Ca_{0.3})TiO_3\}_x$ as well as ($x = 0.20$) to the C–R–T triple point in the phase diagram of $\{Ba(Zr_{0.15}Ti_{0.85})O3\}_{(1-x)}\{(Ba_{0.80}Ca_{0.2})TiO_3\}_x$, but these values are less than the MPB compositions due to polarization instability [8, 9, 13, 21]. Dielectric constant values decrease with increase in frequency, which are due to decrease in polarization with increase in frequency, high values of dielectric constant at low frequencies are due to the presence of various types of polarizations (electronic, ionic, dipolar, and interfacial polarizations) present in the compound, whereas at higher frequencies interfacial, dipolar, and ionic/atomic become insignificant and only electronic polarization dominates and interfacial and dipolar polarizations are temperature dependent thus the dielectric constant becomes lower with increasing frequency [22, 23]. Figure 3 displays the room temperature *P–E* hysteresis loops of BZT–BCT ceramics at a maximum electric field of 80 kV/cm. Well-saturated slender ferroelectric hysteresis *P–E* loops are obtained under the maximum electric field (80 kV/cm) before the dielectric breakdown occurs. Saturation polarization (P_s) of the BZT–BCT ceramics were ~27.17, 36, 22 μC/cm^2 and remnant polarization (P_r) ~8.5, 8.3, 6 μC/cm^2 for $x = 0.1$, 0.15, and 0.20, respectively. Maximum polarization or the saturation polarization (P_s) values are comparably higher than the MPB compositions [24]. Coercive field (E_c) values are 1.46, 0.252, and −0.252 kV/cm for the compositions $x = 0.10$–0.20, these low E_c with higher dielectric constant values manifest that these materials are very soft [8]. The coercive field slightly increases from −0.252 to 1.46 kV/cm and then drastically decreased, and these values are comparably low due to lower breakdown voltage than the MPB compositions, as well as softer than the MPB compositions [24]. Increased polarization values are due to enhanced grain growth and increase in domain size at higher sintering

temperature [25, 26]. Increased spontaneous polarization values ($P_s \sim 27.17$, 36, and 22 μC/cm^2) of present BZT–BCT compositions are higher than those of the MPB composition of BZT–BCT ceramics and thin films (14.1 μC/cm^2) [27]. And as well these enhanced ferroelectric properties for present BZT–BCT compositions were attributed to higher sintering temperature, when compared to lower sintering sol–gel synthesized $(1 - x)$BZT–xBCT ceramics ($P_s \sim 6.56$, 5.71, 1.85 μC/cm^2) [18]. Ferroelectric results are in good agreement with the measurements of the dielectric constant with temperature curves, as shown in Fig. 2 at different frequencies. The strain–electric-field hysteresis loops of BZT–BCT ceramics obtained at room temperature (300 K) by applying an electric field of ~80 kV/cm are shown in Fig. 3 (inset). Symmetric nature of butterfly strain–electric-field loops suggests the piezoelectric nature of the BZT–BCT ceramics. A maximum strain of ~12 % has been observed for the compositions with $x = 0.15$, which might be useful in piezoelectric actuator applications. Typical "butterfly-shaped" hysteresis loop of a sample with preset polarization can be observed in BZT–BCT ceramics: after an initial low value, the strain then makes a steep increase until the maximum filed of around 80 kV/cm (dielectric breakdown was typically observed above this field), and then decreases again to a remanent value as the field is released; the same behavior is exhibited for negative polarity fields. This behavior is commonly connected to switching and movement of domain walls by an applied electric field, similar to that in other ferroelectric materials, particularly for non-180° domain walls, which may involve a significant change in the dimensions of the grains in the ceramics [28].

The room temperature electrical breakdown voltages measured using Trek high voltage amplifier for 0.5-mm thick BZT–BCT ceramic pellets and of which breakdown fields were 140, 170, and 134 kV/cm. The energy density (E_d) of a capacitor is calculated from the P–E hysteresis loop. The energy density is the integral area of the P–E loop (charge—lower branch of P–E curve or discharged curve—upper branch of P–E curve) and y-axis is given by $E_d = \int E dP$, here E is applied electric field and P is the polarization. The ratio of discharge energy density (J_d) to that of the charge energy density (J_c) can be used to evaluate the energy efficient ($\eta = J_d/J_c$) and to analyze the energy storage mechanism of the dielectric materials [29]. Compositional-dependent charging, discharging, and energy storage efficiency of BZT–BCT ceramics are shown in Fig. 4a. The energy storage density is related to dielectric permittivity and dielectric breakdown voltage and it is necessary that electric breakdown voltage should be as high as possible [30]. If excess voltage is applied then the dielectric constant decreases markedly and which in turn decreases the energy storage density [31, 32]. The

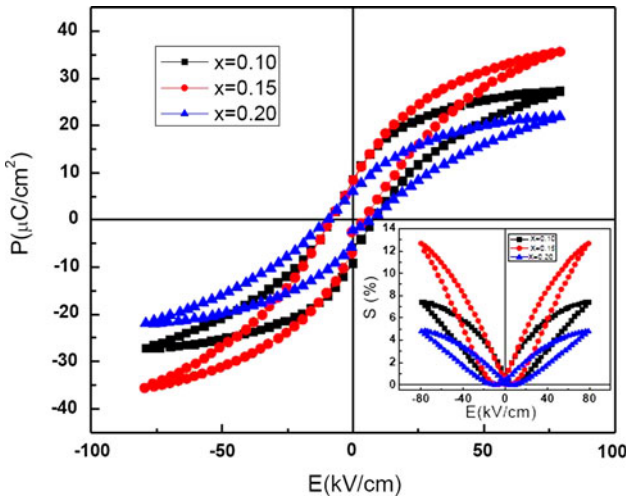

Fig. 3 Room temperature P–E and S–E loops (*inset*) of $[(BaZr_{0.2}Ti_{0.80})O_3]_{(1-x)}$–$[(Ba_{0.70}Ca_{0.30})TiO_3]_x$ ($x = 0.10$, 0.15, 0.20)—(BZT–BCT) ceramics sintered at 1600 °C

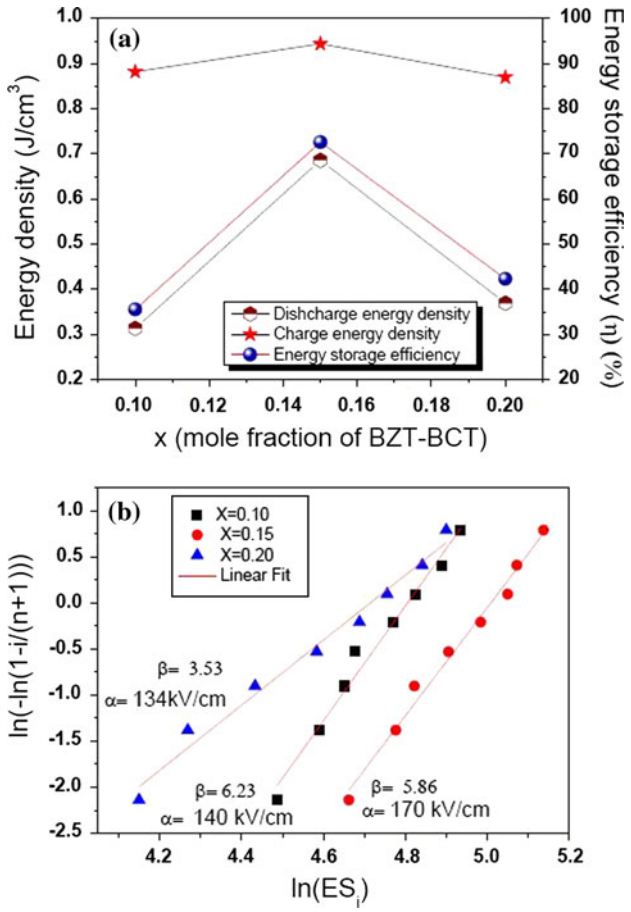

Fig. 4 **a** Composition dependence of discharge energy density (J_d), charge energy density (J_c), and energy storage efficiency (η %) of $[(BaZr_{0.2}Ti_{0.80})O_3]_{(1-x)}$–$[(Ba_{0.70}Ca_{0.30})TiO_3]_x$ ($x = 0.10$, 0.15, 0.20)—(BZT–BCT) ceramics. **b** Weibull plots of the breakdown strength of $[(BaZr_{0.2}Ti_{0.80})O_3]_{(1-x)}$–$[(Ba_{0.70}Ca_{0.30})TiO_3]_x$ ($x = 0.10$, 0.15, 0.20)—(BZT–BCT) ceramics sintered at 1600 °C

Table 1 Room temperature dielectric constant, dielectric breakdown field, and discharge energy density (J_d), charge energy density (J_c), and energy storage efficiency (η %) of $[(BaZr_{0.2}Ti_{0.80})O_3]_{(1-x)}$–$[(Ba_{0.70}Ca_{0.30})TiO_3]_x$ ($x = 0.10, 0.15, 0.20$)—(BZT–BCT) ceramics sintered at 1600 °C

Composition	Dielectric constant (RT-300 K)	Breakdown filed (kV/cm)	Discharge energy density J_d (J/cm^3)	Charge energy density J_c (J/cm^3)	Energy storage efficiency (%) ($\eta = J_d/J_c$)
$[(BaZr_{0\ 2}Ti_{0.80})O_3]_{0.9}[(Ba_{0\cdot 70}Ca_{0.30})TiO_3]_{0.1}$	7800	140	0.31	0.88	35
$[(BaZr_{0\ 2}Ti_{0\ 80})O_3]_{0.85}[(Ba_{0\ 70}Ca_{0.30})TiO_3)_{0.15}$	8400	170	0.68	0.94	72
$[(BaZr_{0\ 2}Ti_{0\ 80})O_3]_{0.8}[(Ba_{0\ 70}Ca_{0.30})TiO_3)_{0.2}$	5200	134	0.36	0.87	42

experimentally obtained room temperature dielectric constant, dielectric breakdown field, and calculated energy densities from *P–E* loops are shown in Table 1. For the mentioned compositions charge energy densities (0.88, 0.94, 0.87 J/cm^3) were comparatively little higher than the discharge energy densities (0.31, 0.68, 0.36 J/cm^3), and of which energy storage efficiencies are 35, 72, and 42 %, respectively. For both charging and discharging cycles, energy density increased as the composition increased from $x = 0.10$ to 0.15 and then decreased to $x = 0.20$, energy storage efficiency also followed the same trend. High dielectric constant, high breakdown strength, low loss, and pore-free dense microstructures are necessary for materials that are to be utilized in high energy density capacitor applications. Calculated energy densities are comparably higher than the other ceramics and glass-mixed ceramics [18, 33–36]. Generally, Weibull statistics were used for failure breakdown analysis using cumulative distribution function [7]. Weibull plots are used to interpret dielectric breakdown field strength (DBS) data and on average minimum 8–10 samples were tested for breakdown measurements. The empirical two-parameter (α, β) Weibull function for failure probability distribution calculated using the relations as mentioned in Ref. [7]. DBS results (with scale parameter α and shape parameter β) are shown in Fig. 4b. The dielectric breakdown field data of all BZT–BCT ceramic samples sintered at 1600 °C follows the two-parameter Weibull distribution, and all the plots show good linearity. The *X*-intercept ln(α), relates to the magnitude of the breakdown strength; and the shape parameter β, which determines the range of DBS, which is calculated from the slope of the Weibull plots. From the Weibull distribution fitting adjusted R^2 values for the mentioned compositions were 0.979, 0.985, and 0.981 and of which shape parameter β were 3.53, 6.23, and 5.86, respectively. Among the present BZT–BCT ceramic compositions, $[(BaZr_{0.2}Ti_{0.80})O_3]_{0.85}$–$[(Ba_{0.70}Ca_{0.30})TiO_3]_{0.15}$ ($x = 0.15$) demonstrated higher dielectric breakdown strength and larger energy densities with high energy storage efficiency ($\eta = 72$ %) than that of the other two compositions. The study may be useful in the fabrication of high energy density capacitor device composed of solid solution BZT–BCT materials.

Conclusions

In conclusion based on the experimental observations, Pb-free BZT–BCT system with dense microstructure is designed at higher sintering temperature. High dielectric constant (ε_r) ~8400 and low loss (tan δ) ~0.014 were obtained at higher sintering temperature (1600 °C) with moderate dielectric breakdown fields. Larger energy densities with high energy storage efficiencies were obtained for BZT–BCT ceramics. Optimizing intrinsic and extrinsic parameters (composition, bulk structure defect chemistry, microstructural development, thickness, electrode configuration, and grain size and) will further improve dielectric breakdown and enhance energy densities in making commercially viable energy storage devices. The *P–E* hysteresis and piezoelectric *S–E* loops of the BZT–BCT ceramics have shown very good ferroelectric and piezoelectric behavior. These results confirm the successful preparation of a BZT–BCT bulk ceramics with ferroelectric and piezoelectric behavior might be useful in actuator applications. The present BZT–BCT ceramics with interesting dielectric, ferroelectric, and piezoelectric hysteresis properties, stimulates interests in developing BZT–BCT thin films for wide range of capacitors for energy storage applications.

Acknowledgements This study was supported by the National Science Foundation under Grant No. NSF-EFRI # 1038272. The authors are also thankful to Cristina Diaz Borrero, Material Characterization Center, University of Puerto Rico for doing SEM measurements. Author Venkata S. Puli thank D. Kishore Kumar, Department of chemistry, UPR, RP, for useful discussions.

References

1. Chu B, Zhou X, Ren K, Neese B, Lin M, Wang Q, Bauer F, Zhang QM (2006) Science 313(5785):334
2. Slenes KM, Winsor P, Scholtz T, Hudis M (2001) IEEE Trans Magn 37:324

3. Ogihara H, Randall CA, Trolier-McKinstry S (2009) J Am Ceram Soc 92(8):1719
4. Karan NK, Saavedra-Arias JJ, Perez M, Thomas R, Katiyar RS (2008) Appl Phys Lett 92:012903
5. Chen X, Zhang H, Cao F, Wang G, Dong X, Yan G (2009) J Appl Phys 106:034105
6. Ma B, Narayanan M, Balachandran U (2009) Mater Lett 63:1353
7. Ma B, Tong S, Narayanan M, Liu S, Chao S, Balachandran U (2011) Mater Res Bull 46:1124
8. Liu W, Ren X (2009) Phys Rev Lett 103:257602
9. Xue D, Zhou Y, Bao H, Gao J, Zhou C, Ren X (2011) Appl Phys Lett 99:122901
10. Dixit A, Majumder SB, Dobal PS, Katiyar RS, Bhalla AS (2004) Thin Solid Films 447–448:284
11. Choudhury S, Bhuiyan MA, Hoque SM (2011) Int Nano Lett 1(2):111
12. Chen T-Y, Chu S-Y, Juang Y-D (2002) Sens Actuators A 102:6
13. Bao H, Zhou C, Xue D, Gao J, Ren X (2010) J Phys D Appl Phys 43:465401
14. Shrout TR, Zhang SJJ (2007) Electroceramics 19:111
15. Takenaka T, Nagata HJ (2005) Eur Ceram Soc 25:2693
16. Chen X, Ma HY, Ding W, Zhang Y, Zhao X, Lian X, Liu P (2011) J Am Ceram Soc 94(10):3364
17. Victor P, Ranjith R, Krupanidhi SB (2003) J Appl Phys 94(12):7702
18. Puli VS, Kumar A, Chrisey DB, Tomozawa M, Scott JF, Katiyar RS (2011) J Phys D Appl Phys 44:395403
19. Palei PK, Kumar P (2012) J Appl Phys 51:011503
20. Lee HS, Kimura T (1998) J Am Ceram Soc 81(12):3228
21. Zhou C, Liu W, Xue D, Ren X, Bao H, Gao J, Zhang L (2012) Appl Phys Lett 100:222910
22. Sen S, Choudhary RNP (2004) J Mater Sci Mater Electron 15:671
23. Singh AK, Goel TC, Mendiratta RG, Thakur OP, Prakash C (2002) J Appl Phys 91(10):6626
24. Ehmke MC, Ehrlich SN, Blendell JE, Bowman KJ (2012) J Appl Phys 111:124110
25. Cao W, Randall CA (1996) J Phys Chem Solids 57(10):1499
26. Smolenskii GA, Iagranovskaya A (1958) Sov Phys Tech Phys 3:1380
27. Piorra A, Petraru A, Kohlstedt H, Wuttig M, Quandt E (2011) J Appl Phys 109:104101
28. Uchino K (2000) Ferroelectric devices. Marcel Dekker, New York
29. Pan J, Li K, Li J, Hsu T, Wang Q (2009) Appl Phys Lett 95:022902
30. Yao K, Chen S, Rahimabady M, Mirshekarloo MS, Yu S, Tay FEH, Sritharan T, Lu L (2011) IEEE Trans Ultrason Ferroelectr Freq Control 58(9):1968
31. Ricketts BW, Triani G, Hilton AD (2000) J Mater Sci Mater Electron 11(6):513
32. Dong G, Ma S, Jun D, Cui J (2009) Ceram Int 35:2069
33. Puli VS, Pradhan DK, Kumar A, Su X, Busta CM, Tomozawa M, Chrisey DB, Katiyar RS (2012) J Mater Sci Mater Electron. doi:10.1007/s10854-012-0694-9
34. Puli VS, Kumar A, Su X, Busta CM, Tomozawa M, Chrisey DB, Katiyar RS (2012) J Non Cryst Solids. doi:10.1016/j.jnoncrysol.2012.05.018
35. Zhou Y, Zhang Q, Luo J, Tang Q, Jun D (2011) Scripta Mater 65:296
36. X Wang, Y Zhang, T Ma, Z Yuan, Q Zhang, C Deng, T Liang (2012) Int Appl Ceram Technol 1–6. doi:10.1111/j.1744-7402.2011.02733.x